

# Gyromorphs: a new class of functional disordered materials

Mathias Casiulis,<sup>1,2,\*</sup> Aaron Shih,<sup>3,1,\*</sup> and Stefano Martiniani<sup>3,1,2,†</sup>

<sup>1</sup>Center for Soft Matter Research, Department of Physics, New York University, New York 10003, USA

<sup>2</sup>Simons Center for Computational Physical Chemistry, Department of Chemistry, New York University, New York 10003, USA

<sup>3</sup>Courant Institute of Mathematical Sciences, New York University, New York 10003, USA

(Dated: October 14, 2024)

We introduce a new class of functional correlated disordered materials, termed Gyromorphs, which uniquely combine liquid-like translational disorder with quasi-long-range rotational order, induced by a ring of  $G$  delta peaks in their structure factor. We generate gyromorphs in  $2d$  and  $3d$  by spectral optimization methods, verifying that they display strong discrete rotational order but no long-range translational order, while maintaining rotational isotropy at short range for sufficiently large  $G$ . We show that they are distinct from quasicrystals, which we argue are akin to Fourier “duals” of gyromorphs. Using a coupled dipoles approximation, we show that these structures outperform quasicrystals, stealthy hyperuniformity, and Vogel spirals in the formation of isotropic bandgaps in  $2d$ , for both scalar and vector waves, and open complete isotropic bandgaps in  $3d$ . Finally, we introduce “polygyromorphs” with several rotational symmetries at different length scales (i.e., multiple rings of delta peaks), enabling the formation of multiple bandgaps in a single structure, thereby paving the way for fine control over optical properties.

A crucial aspect of the design and discovery of new materials is understanding the relationship between structure and properties. Crystals have proven to be a highly versatile platform for engineering functions, as the periodicity of their atomic arrangement greatly facilitates the prediction and optimization of their properties. However, not all properties can be realized with periodic structures. Aperiodic media can achieve transport properties unattainable in periodic systems, such as the formation of isotropic photonic bandgaps, which are highly desirable in optoelectronic applications such as freeform waveguides [1, 2] and tunable-reflectance coatings [3]. While isotropic bandgaps have been demonstrated in some deterministic aperiodic systems such as Vogel spirals [4–8], and near-isotropic bandgaps have been observed in quasicrystals [9–11], many recent works have sought this property in correlated disordered structures [12, 13], *i.e.* random point patterns that lack conventional long-range order but exhibit spatial correlations.

Unlike in periodic systems, the structural origins of photonic bandgaps – or more precisely, “pseudogaps”, characterized by a depletion in the density of states relative to vacuum, leading to reduced transmission [14, 15] – remain poorly understood in aperiodic systems. Disordered stealthy hyperuniform (SHU) structures [16], which suppress density fluctuations over long distances, have been shown to exhibit isotropic bandgaps in both  $2d$  and  $3d$  [14, 15, 17–22], but only when strong short-range correlations are also present [14, 15, 17, 23–25]. Further complicating the picture, photonic bandgaps have also been observed in non-SHU disordered structures, such as jammed packings [26–28], and even in systems with only short-range correlations, like equilibrium hard spheres [29], which are not hyperuniform. The role of short range correlations in disordered systems is especially pronounced for vector waves, for which bandgaps

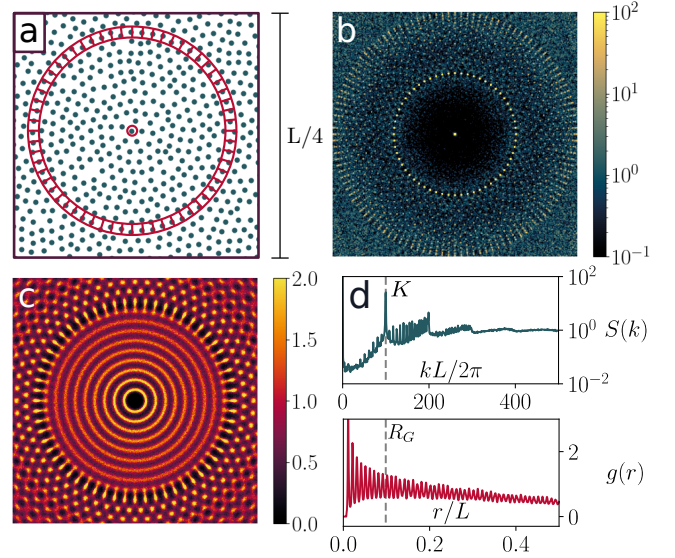


FIG. 1. **Introducing: Gyromorphs.** (a) Section of the point pattern of a 60-fold gyromorph. We show the shortest distance displaying 60-fold order. (b) Corresponding structure factor. (c) Corresponding pair correlation function  $g(\mathbf{r})$  near the origin. (d) Structure factor  $S(k)$  (top) and radial distribution function  $g(r)$  (bottom) for the 60-fold gyromorph.

have so far only been observed in networked materials, such as honeycomb or tetrahedrally bonded structures [10, 17, 27, 30, 31]. In these random networks, the emergence of bandgaps has been linked to the similarity of local geometry and topology across the network [23, 27, 30].

This raises the question: is there a unifying feature across these systems that promotes the formation of isotropic photonic bandgaps? In the single-scattering regime, the emergence of a bandgap can be attributed to the presence of strong scattering at some characteristic frequency, and of weaker scattering at neighboring

frequencies. This argument has been invoked to justify the appearance of bandgaps in quasicrystals [11, 32–34], and explains why bandgaps also arise in systems with short-range correlations, such as equilibrium hard sphere liquids [29, 35]. In fact, we observe that all previously cited aperiodic systems that exhibit isotropic bandgaps have an isotropic ring of high values in their structure factor,  $S = |\hat{\rho}(\mathbf{k})|^2/N$ , where  $\rho(\mathbf{r})$  is the density field defining the system. This condition is also well approximated by quasicrystals, whose most intense structure factor peaks form regular polygons [36, 37].

Bravely adhering to this single-scattering rationale, an ideal bandgap material should exhibit a ring of high values in  $S(k)$ , contrasting with low values around it. Accordingly, we propose a correlated disordered structure whose structure factor displays one ring of  $G \in 2N^*$  delta peaks with intensities  $\mathcal{O}(N)$  on a circle with radius  $K$ , but as little order as possible elsewhere. In this work, we show that such hypothetical structures, which we call *gyromorphs*, are realizable, and we present a reliable algorithm for their generation in  $2d$  and  $3d$ .

In gyromorphs, liquid-like translational disorder coexists with a ring of extensive peaks, resulting in quasi-long-range rotational order. These structures are thus fundamentally distinct from any previously known materials, as they reconcile seemingly contradictory features. We successfully generate finite gyromorphs with up to  $G \sim 10^3$  peaks, whose heights surpass the peak intensities of finite quasicrystals obtained by usual deterministic methods [38, 39] (see Appendix). Remarkably, we uncover a duality between the structure factor and pair correlation functions of gyromorphs and quasicrystals, suggesting that, at high rotational symmetries, gyromorphs may outperform quasicrystals as bandgap materials. Using a coupled dipoles approximation [40–42], we thus demonstrate that gyromorphs outmatch previous candidate systems in  $2d$  as isotropic bandgap materials, for both vector and scalar waves [37]. Finally, we demonstrate that gyromorphs can be extended to  $3d$  structures exhibiting *complete* isotropic bandgaps, as well as to “polygyromorphs” with multiple rings of peaks, resulting in multiple bandgaps in a single system.

*Generating gyromorphs* – To generate gyromorphs, we use the Fast Reciprocal-Space Correlator (FReSCo) [35]. We use the NUwNU (non-uniform real space with non-uniform  $k$ -space constraints) variant, which imposes constraints at continuous reciprocal space positions, assuming free boundary conditions for the point pattern. Starting from an initially uncorrelated random point pattern with  $N$  points, we optimize it to display  $G$  high peaks (each with target height  $N$ ) regularly spaced on a ring, thereby creating a  $G$ -fold gyromorph (see SM [37]).

*Structure of gyromorphs* – At high  $G$ , although the point pattern appears isotropic at short length scales, gyromorphs still exhibit strong  $G$ -fold order at large length scales, as shown in Fig. 1. In Fig. 1(a), we show a portion

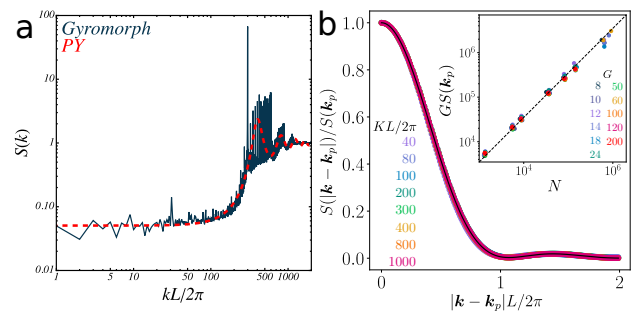


FIG. 2. **Order in gyromorphs.** (a)  $S(k)$  of a 60-fold gyromorph (blue) with  $N \sim 10^5$  ( $KL/2\pi = 300$ ), compared to a Percus-Yevick  $S(k)$  for  $\phi = 0.57$  (dashed red line) in log scales. (b) Corresponding radially averaged profile of peaks across  $K$  values, rescaled by peak height (colored lines) a solid black line indicates the radial profile of  $\text{sinc}^2(k_x L/2)\text{sinc}^2(k_y L/2)$ . Inset: Rescaled peak height  $GS(\mathbf{k}_p)$  against  $N$ , in log scales, for  $KL/2\pi = 300$  across  $G$  (colored symbols). A dashed black line shows  $GS(\mathbf{k}_p) = 3.5N$ .

of an  $N \sim 10^4$ ,  $G = 60$  gyromorph, highlighting in red the “gear” with radius  $R_G \approx G/K$  [37] onto which 60-fold order is first achieved around an example point. Note that this is different from bond-orientational order [43], which describes nearest-neighbor ordering only; at high  $G$ , gyromorphs have no such order, unlike quasicrystals. In Fig. 1(b), we show the corresponding structure factor, highlighting a strong 60-fold ring of peaks, that are intense enough to display a few echoes, and low-intensity regions around the peaks. In Fig. 1(c), we show the central part of the corresponding pair correlation function  $g(\mathbf{r})$ . This function illustrates that each particle is surrounded by the gear of Fig. 1(a), with the same orientation, at the smallest ring of neighbors capable of accommodating  $G$ -fold order [37]. Additionally, it reveals that, at shorter distances, the local neighborhoods are perfectly isotropic. The short-range “disorder” is highlighted in Fig. 1(d) by the radial plots of  $S(k)$  (top) and  $g(r)$  (bottom). While  $S$  is peaked at  $K$  and shows a few nearby echoes, it eventually decays to 1 at larger  $k$ , indicating the absence of short-range order. Similarly,  $g$  is notably less peaked than that of (quasi)crystalline structures, exhibiting no visible feature at  $R_G$ , and decaying with increasing distance. Overall, Fig. 1 highlights that  $S - 1$  is essentially just a  $G$ -fold ring of Dirac deltas, so that the  $g(r)$  is well approximated by a sum of cosines akin to “kaleidoscopic” optical fields obtained by holographic techniques [44, 45]. In contrast, quasicrystals display rings of peaked  $g$  corresponding to a discrete set of allowed neighbor positions [38, 39], so that  $S$  is well approximated by a sum of cosines at high  $G$ . This “Fourier duality” between gyromorphs and quasicrystals is illustrated in Appendix.

To further investigate the nature of order in gyromorphs, we replot a structure factor in log-log scales in

Fig. 2(a). This panel shows that gyromorphs are *not* hyperuniform, as the low- $k$  limit of  $S$  saturates at a level similar to that of a Percus-Yevick model for equilibrium hard disk liquids [46]. We further validate this observation by measuring local number fluctuations in real space over windows of increasing size [16, 35] (see Appendix), finding that the long-range density fluctuation scaling of gyromorphs is indistinguishable from that of hard disks. Furthermore, at large  $k$ , the decay of  $S(k)$  is also similar to that of a liquid. These results suggest that, with respect to translational order, gyromorphs are more akin to liquids than to quasicrystals.

In Fig. 2(b), we analyze the peaks. In the main panel, we show the profile of the peak at  $(KL/2\pi, 0)$ , normalized by its height, as a function of the distance  $kL/2\pi$  to the maximum, across system sizes for  $G = 60$ . As  $N$  grows, the profile converges to  $\text{sinc}^2(kL/2)$ , implying that the linear width of the peaks in  $k$ -space decays like  $1/L$ . The inset shows that, for different values of  $G$ , the peak heights grow like  $O(GN)$ , indicating that the peaks are extensive for any fixed order symmetry. Altogether, the peaks have extensive height while their area decays like  $1/L^2 \sim 1/N$ : they approach Dirac deltas as  $N$  increases, like in quasicrystals, so that gyromorphs display quasi-long-range rotational order (see Appendix).

*Coupled Dipoles Method* – We now turn our attention to the optical properties of gyromorphs. From an Ewald-sphere construction [47, 48] one expects a ring of many high peaks at radius  $K$  to generate strong backscattering at  $K/2$  [33]. That is why quasicrystals were deemed good candidates for isotropic bandgaps. However, they display increasingly shallow bandgaps as their order of rotational symmetry grows [10], which can be attributed to weakening features in  $S$  in de Bruijn’s construction [38, 39] as  $G$  increases. By contrast, gyromorphs are only constrained to display a finite set of high fine peaks, and they may retain a deep isotropic bandgap even at high  $G$ .

To verify this, we assume that each point in the gyromorph represents a non-magnetic scatterer with a dielectric contrast  $\delta\varepsilon(\omega) \in \mathbb{C}$  from the surrounding medium at pulsation  $\omega$ , corresponding to a refractive index  $n = \sqrt{1 + \delta\varepsilon}$ , and a radius  $a$ . Limiting our analysis to wavevectors  $k_0 = \omega/c$  (with  $c$  the celerity of waves in the host medium) such that  $k_0 a \ll 1$  (Rayleigh scattering [42]), we employ a coupled dipoles approximation to describe the scattering of waves by the structure. This standard method [40–42] turns the problem of solving Maxwell’s equations in the medium (a very strenuous task that involves a full discretization of space as well as very specific choices of boundary conditions [49, 50]) into a linear system, see Appendix. In short, setting only  $a$  and  $n$  for the scatterers, we measure transmitted intensities for any choice of monochromatic source field, as well as an integrated local density of optical states (LDOS). Throughout the main text, we present results for vector waves (Transverse Electric, or TE, mode in  $2d$ , as opposed to

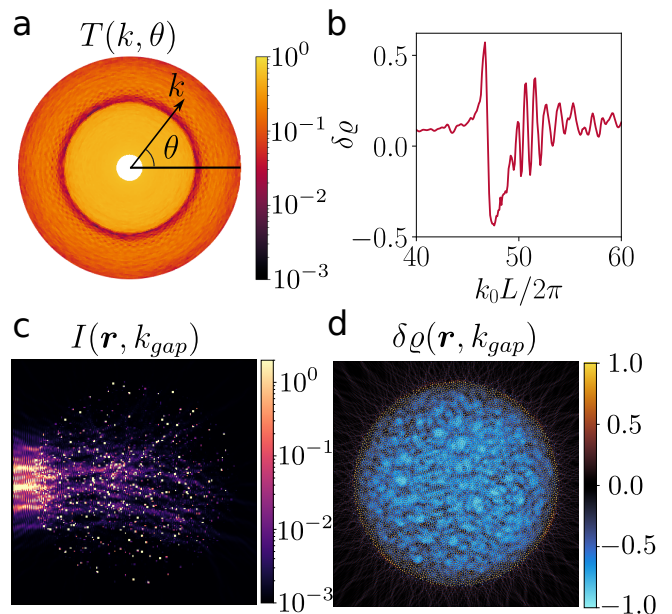


FIG. 3. **Optical properties of gyromorphs** We use an example 60-fold gyromorph and focus on TE polarization. (a) Intensity transmission for frequencies  $40 \leq k_0 L / 2\pi \leq 60$  (radial direction) and 360 incident angles (orthoradial direction) of a source Gaussian beam. (b) Relative LDOS change with respect to vacuum, averaged over 1000 random points, highlighting a dip close to  $k_0 = K/2$  (here  $KL/2\pi = 100$ ). (c) Spatial map of the intensity at angle 0 and  $k_0 L / 2\pi = 47.6$ , which corresponds to the minimum of both transmission and LDOS. (d) Corresponding LDOS map.

the scalar-wave Transverse Magnetic, or TM, mode). We report the scalar-wave results in SM [37], as scalar-wave bandgaps are less challenging to obtain in point patterns [10, 15, 17, 23]. All optical properties are computed within the Materials Analysis via Green’s Tensors (MAGreeTe) library, which we make publicly available [51].

*Existence of a bandgap* – First, in Fig. 3, we focus on a single  $2d$  gyromorph with  $G = 60$  and  $N \sim 10^4$  to determine whether a bandgap is present. We first trim the system to a circular shape of radius  $R = L/2$  to avoid any anisotropy due to the overall shape of the medium, like in many experimental tests [9, 17, 18]. We then set the radius  $a$  of scatterers such that the filling fraction  $\phi \equiv Na^2/R^2$  equals 5% and the dielectric contrast  $\delta\varepsilon = 8$  ( $n = 3$  for scatterers in vacuum), a typical value for metal oxides used in experiments [22]. Following Refs. [9, 17, 18, 22], we first perform transmission measurements. We set the source to be a standard Gaussian beam with zero curvature focused at the center of the medium [42, 52, 53]. We solve the coupled dipoles system for 360 regularly spaced orientations  $\theta$  of the beam and for several frequencies  $k_0$ . Then, following Refs. [52], we measure the transmitted intensity behind the system at a distance  $D$  from its nearest edge [54]. For each incoming beam orientation  $\theta$ , we define the transmission as

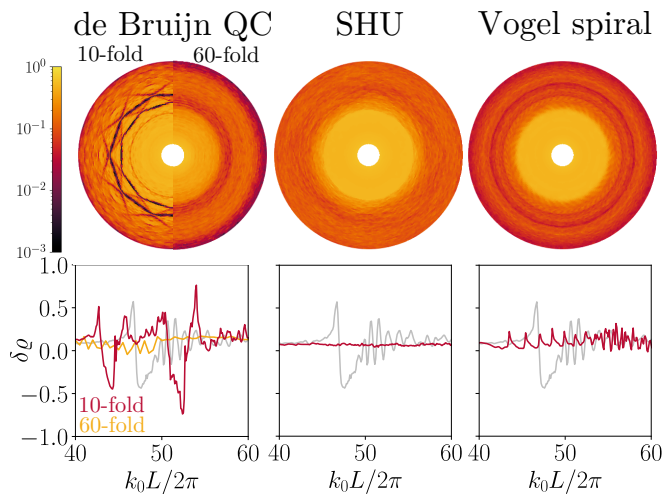


FIG. 4. **Comparison with other systems** Top row: TE intensity transmissions as a function of  $k_0$  (radial) and beam orientation (orthoradial) for (from left to right) 10- and 60-fold de Bruijn quasicrystals, an SHU structure, and a Vogel spiral. Bottom row: Corresponding  $\delta\rho$  (red lines), with the 60-fold gyromorph shown as a light gray line. All results are obtained for  $n = 3$ ,  $\phi = 0.05$ .

the average intensity over 180 angles in  $[\theta - \pi/2; \theta + \pi/2]$  on the half-circle with radius  $D$ , normalized by the value of the incident field at these points in the absence of the medium [37]. The results, shown in Fig. 3(a) in the plane of incident wave-vectors  $(k_0, \theta)$ , display a clear trough of low intensities at  $k_{gap} \lesssim K/2$ , as expected from single-scattering arguments [33, 35]. An intensity map for  $\theta = 0$  and  $k_0 = k_{gap}$  is shown in Fig. 3(c), confirming that the field is strongly backscattered. To confirm that this lower transmission is the sign of a bandgap, we measure the DOS of the system. In Fig. 3(b), we show  $\delta\rho$ , the relative change of DOS compared to vacuum averaged over 1000 random points drawn randomly across the material but at least  $2a$  away from scatterers, following Refs. [14, 55]. We show strong mode depletion at  $k_{gap}L/2\pi = 47.6$ . Finally, a map of the local  $\delta\rho$  across the system in Fig. 3(d) shows consistent mode depletion across the bulk. These results are confirmed by standard but costlier finite-difference methods [49] in small systems in SM [37], where we also show similar TM results.

*Comparison to other systems* – We compare the results of Fig. 3 to classic bandgap candidates, namely 10- and 60-fold deterministic quasicrystals obtained by the de Bruijn’s construction [37–39, 56], a deterministic Vogel spiral [4], and a random SHU structure generated by FReSCo [35] with a degree of stealthiness such that it displays a TM bandgap [14, 15, 17, 18, 21, 29, 37]. Structures are adjusted to contain  $N \sim 10^4$  points and a ring of higher values at the same  $K$  as the gyromorphs, and we set all parameters to the same values as in Fig. 3. We report transmission plots in the top row of Fig. 4, and DOS

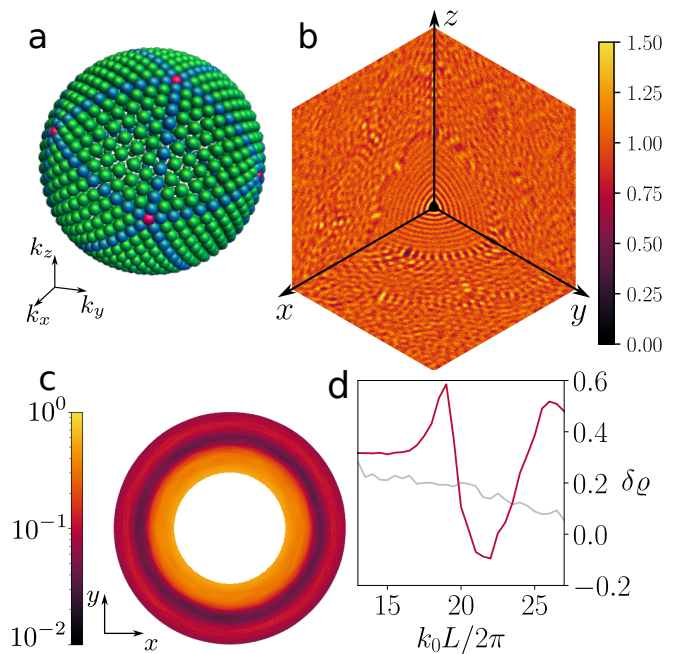


FIG. 5. **Three-dimensional gyromorphs.** (a) 3d-rendered orthographic view of the constrained peaks on the sphere. From an icosahedron (red), we subdivide edges (blue) and faces (green) so as to cover the whole sphere uniformly. (b) Cross-sections (in the  $x = 0$ ,  $y = 0$ , and  $z = 0$  planes) of the  $g(\mathbf{r})$  of a gyromorph with  $G = 1212$ ,  $N = 83762$ . (c) Vector-wave transmission averaged over the forward half-sphere, for a beam source rotating in the  $z = 0$  plane. (d) Radially averaged transmission (top) and relative DOS change (bottom) for the gyromorph (colored lines), compared to a Poisson point pattern (gray lines). In (c), (d), we use a ball of  $N \approx 15000$  points from the structure and set  $\phi = 0.1$ ,  $n = 6.5$ .

in the bottom row. We show that Vogel and SHU systems display much shallower transmission troughs than the gyromorphs, which we attribute to weaker features in  $S(k)$ , and very little DOS change. Furthermore, we show that quasicrystals may either display rather deep but anisotropic gaps at low symmetries, or isotropic but shallow gaps at high symmetry due to the broadening of their  $S(k)$  features [10, 37]. In fact, the bandgaps of finite-size gyromorphs are as deep as in low-order quasicrystals but more isotropic than them at comparable  $\delta\varepsilon$ . We check [37] that the DOS dip in gyromorphs gets deeper with index contrast and system size (following a power law, like in defective crystals or SHU structures [14, 57, 58]), but does not strongly depend on  $G$ .

*Extension to 3d* – We now extend the concept of gyromorphs to 3d structures. We optimize structures to display  $G$  regularly spaced peaks on a sphere with radius  $K$  in their structure factor. As there is no standardized way to populate points evenly spaced on a sphere while preserving centrosymmetry, we choose the location of peaks by building upon icosahedral geometry. Starting from an icosahedron of peaks, we subdivide each icosahed-

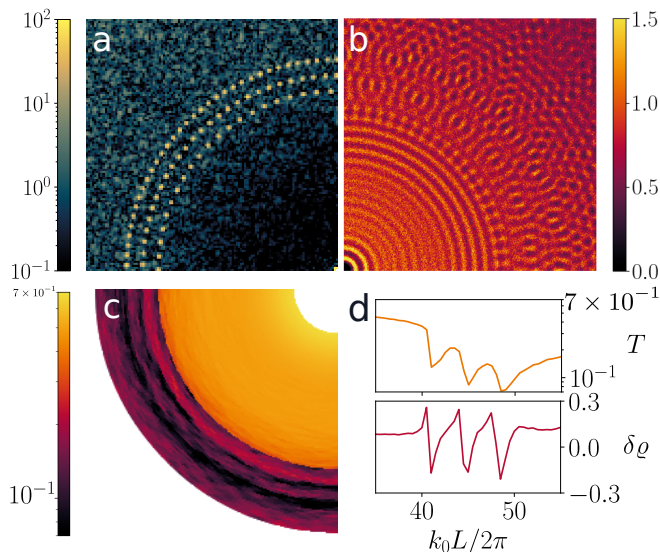


FIG. 6. **Polygyromorphs.** (a) Structure factor featuring 3 rings with 82, 106, and 134 peaks at  $KL/2\pi$  equal to 85, 92.5, and 100 respectively. Corresponding (b)  $g(\mathbf{r})$ , (c) TE transmission, and (d) Radially averaged transmission  $T$  (top) and LDOS relative change (bottom).

dral face into multiple triangular faces and project those additional vertices onto the sphere. An example of such a set of peaks is shown in Fig. 5(a). We show in Fig. 5(b) cross-sections of the  $g(\mathbf{r})$  for a gyromorph thus obtained with  $G \approx 10^3$ . Finally, in Fig. 5(c) – (d), we show optical properties measured for this system, namely a transmission plot and the averaged relative change of LDOS for vector waves. We report an isotropic transmission gap, that is correlated to a depletion of DOS, which shows that 3d gyromorphs are promising bandgap formers.

*Beyond one ring* – Finally, we extend the concept of gyromorphs to disordered systems displaying several rings of peaks. An example system is shown in Fig. 6, where we impose 3 rings of mutually prime (up to parity) rotational orders, at distances with irrational ratios to ensure that the structure is not trivially compatible with a single (quasi)crystal. The resulting structure factor and pair correlation function are shown in Fig. 6(a) and (b), respectively. This structure is expected to display 3 consecutive dips in transmission and DOS, which we indeed report in Fig. 6(c) and (d). This example highlights that gyromorphs are much more general than “dual quasicrystals” and can be used to obtain arbitrary transmission gaps in an aperiodic medium.

*Conclusion* – We introduced a novel class of disordered materials, termed gyromorphs, which are translationally disordered but exhibit one (or several) ring of delta peaks, resulting in quasi-long-range discrete rotational order. We showed that gyromorphs with high rotational order exhibit deeper isotropic bandgaps than systems previously considered in the literature, in both 2d and 3d, and

that several such features can be imposed at once. This advance is significant both fundamentally and practically. Fundamentally, we conceived and verified the existence of a new class of structures that reconciles seemingly contradictory features and stands apart from all known material types. Practically, our numerical predictions indicate that gyromorphs outperform existing isotropic photonic bandgap materials. Gyromorphs thus show promise for applications such as freeform waveguides [1, 2] and lightweight coatings with strong backscattering, such as highly reflective “white” structures [59, 60].

*Acknowledgments* – The authors would like to thank Weining Man, Paul Chaikin, Dov Levine, Rémi Carminati, Luís Froufe-Pérez, Frank Scheffold, and Werner Krauth for insightful comments on this work. A.S., M.C., and S.M. acknowledge the Simons Center for Computational Physical Chemistry for financial support. This work was supported in part through the NYU IT High Performance Computing resources, services, and staff expertise. Parts of the results in this work make use of the colormaps in the CMasher package [61]. Correlations are computed using the rusted\_core library. The FReSCo, MAGreeTe, and rusted-core libraries are publically available [51, 62, 63].

\* Equal contribution.

† sm7683@nyu.edu

- [1] W. Man, M. Florescu, E. P. Williamson, Y. He, S. R. Hashemizad, B. Y. Leung, D. R. Liner, S. Torquato, P. M. Chaikin, and P. J. Steinhardt, Isotropic band gaps and freeform waveguides observed in hyperuniform disordered photonic solids, *Proceedings of the National Academy of Sciences of the United States of America* **110**, 15886 (2013).
- [2] M. M. Milošević, W. Man, G. Nahal, P. J. Steinhardt, S. Torquato, P. M. Chaikin, T. Amoah, B. Yu, R. A. Mullen, and M. Florescu, Hyperuniform disordered waveguides and devices for near infrared silicon photonics, *Scientific Reports* **9**, 20338 (2019).
- [3] P. M. Piechulla, E. Slivina, D. Bätznner, I. Fernandez-Corbaton, P. Dhawan, R. B. Wehrspohn, A. N. Sprafke, and C. Rockstuhl, Antireflective Huygens’ Metasurface with Correlated Disorder Made from High-Index Disks Implemented into Silicon Heterojunction Solar Cells, *ACS Photonics* **8**, 3476 (2021).
- [4] H. Vogel, A Better Way to Construct the Sunflower Head, *Mathematical Biosciences* **44**, 179 (1979).
- [5] M. E. Pollard and G. J. Parker, Low-contrast bandgaps of a planar parabolic spiral lattice, *Optics Letters* **34**, 2805 (2009).
- [6] S. F. Liew, H. Noh, J. Trevino, L. D. Negro, and H. Cao, Localized photonic band edge modes and orbital angular momenta of light in a golden-angle spiral, *Optics InfoBase Conference Papers* **19**, 23631 (2012).
- [7] J. Trevino, S. F. Liew, H. Noh, H. Cao, and L. Dal Negro, Geometrical structure, multifractal spectra and localized optical modes of aperiodic Vogel spirals, *Optics Express*

- 20**, 3015 (2012).
- [8] L. A. Razo-López, G. J. Aubry, F. A. Pinheiro, and F. Mortessagne, Strong localization of microwaves beyond two dimensions in aperiodic Vogel spirals, *Physical Review B* **109**, 014205 (2024).
- [9] W. Man, M. Megens, P. J. Steinhardt, and P. M. Chaikin, Experimental measurement of the photonic properties of icosahedral quasicrystals, *Nature* **436**, 993 (2005).
- [10] M. C. Rechtsman, H. C. Jeong, P. M. Chaikin, S. Torquato, and P. J. Steinhardt, Optimized structures for photonic quasicrystals, *Physical Review Letters* **101**, 073902 (2008).
- [11] Z. V. Vardeny, A. Nahata, and A. Agrawal, Optics of photonic quasicrystals, *Nature Photonics* **7**, 177 (2013).
- [12] S. Yu, C. W. Qiu, Y. Chong, S. Torquato, and N. Park, Engineered disorder in photonics, *Nature Reviews Materials* **6**, 226 (2021).
- [13] K. Vynck, R. Pierrat, R. Carminati, L. S. Froufe-Pérez, F. Scheffold, R. Sapienza, S. Vignolini, and J. J. Sáenz, Light in correlated disordered media, *Reviews of Modern Physics* **95**, 045003 (2023).
- [14] L. S. Froufe-Pérez, M. Engel, J. J. Sáenz, and F. Scheffold, Band gap formation and Anderson localization in disordered photonic materials with structural correlations, *Proceedings of the National Academy of Sciences of the United States of America* **114**, 9570 (2017).
- [15] R. Monsarrat, R. Pierrat, A. Tourin, and A. Goetschy, Pseudogap and Anderson localization of light in correlated disordered media, *Physical Review Research* **4**, 033246 (2022).
- [16] S. Torquato, Hyperuniform states of matter, *Physics Reports* **745**, 1 (2018).
- [17] M. Florescu, S. Torquato, and P. J. Steinhardt, Designer disordered materials with large, complete photonic band gaps, *Proceedings of the National Academy of Sciences of the United States of America* **106**, 20658 (2009).
- [18] W. Man, M. Florescu, K. Matsuyama, P. Yadak, G. Nahal, S. Hashemizad, E. Williamson, P. Steinhardt, S. Torquato, and P. Chaikin, Photonic band gap in isotropic hyperuniform disordered solids with low dielectric contrast, *Optics Express* **21**, 19972 (2013).
- [19] N. Muller, J. Haberko, C. Marichy, and F. Scheffold, Silicon hyperuniform disordered photonic materials with a pronounced gap in the shortwave infrared, *Advanced Optical Materials* **2**, 115 (2014).
- [20] S. Tsitrin, E. P. Williamson, T. Amoah, G. Nahal, H. L. Chan, M. Florescu, and W. Man, Unfolding the band structure of non-crystalline photonic band gap materials, *Scientific Reports* **5**, 13301 (2015).
- [21] M. A. Klatt, P. J. Steinhardt, and S. Torquato, Wave propagation and band tails of two-dimensional disordered systems in the thermodynamic limit, *Proceedings of the National Academy of Sciences of the United States of America* **119**, e2213633119 (2022).
- [22] L. Siedentop, G. Lui, G. Maret, P. M. Chaikin, P. J. Steinhardt, S. Torquato, P. Keim, and M. Florescu, Stealthy and hyperuniform isotropic photonic bandgap structure in 3D, *Arxiv Preprint*, 2403.08404 (2024), arXiv:2403.08404.
- [23] M. Florescu, S. Torquato, and P. J. Steinhardt, Complete band gaps in two-dimensional photonic quasicrystals, *Physical Review B - Condensed Matter and Materials Physics* **80**, 155112 (2009).
- [24] Y. Zheng, L. Liu, H. Nan, Z. X. Shen, G. Zhang, D. Chen, L. He, W. Xu, M. Chen, Y. Jiao, and H. Zhuang, Disordered hyperuniformity in two-dimensional amorphous silica, *Science Advances* **6**, eaba0826 (2020).
- [25] L. S. Froufe-Pérez, G. J. Aubry, F. Scheffold, and S. Magkiriadou, Bandgap fluctuations and robustness in two-dimensional hyperuniform dielectric materials, *Optics Express* **31**, 18509 (2023).
- [26] J. K. Yang, C. Schreck, H. Noh, S. F. Liew, M. I. Guy, C. S. O'Hern, and H. Cao, Photonic-band-gap effects in two-dimensional polycrystalline and amorphous structures, *Physical Review A - Atomic, Molecular, and Optical Physics* **82**, 053838 (2010).
- [27] S. F. Liew, J. K. Yang, H. Noh, C. F. Schreck, E. R. Dufresne, C. S. O'Hern, and H. Cao, Photonic band gaps in three-dimensional network structures with short-range order, *Physical Review A - Atomic, Molecular, and Optical Physics* **84**, 063818 (2011).
- [28] K. Djeghdi, U. Steiner, and B. D. Wilts, 3D Tomographic Analysis of the Order-Disorder Interplay in the Pachyrhynchus congestus mirabilis Weevil, *Advanced Science* **9**, 2202145 (2022).
- [29] L. S. Froufe-Pérez, M. Engel, P. F. Damasceno, N. Muller, J. Haberko, S. C. Glotzer, and F. Scheffold, Role of Short-Range Order and Hyperuniformity in the Formation of Band Gaps in Disordered Photonic Materials, *Physical Review Letters* **117**, 1 (2016).
- [30] S. R. Sellers, W. Man, S. Sahba, and M. Florescu, Local self-uniformity in photonic networks, *Nature Communications* **8**, 14439 (2017).
- [31] M. A. Klatt, P. J. Steinhardt, and S. Torquato, Phoamtonic designs yield sizeable 3D photonic band gaps, *Proceedings of the National Academy of Sciences of the United States of America* **116**, 23480 (2019).
- [32] Y. S. Chan, C. T. Chan, and Z. Y. Liu, Photonic band gaps in two dimensional photonic quasicrystals, *Physical Review Letters* **80**, 956 (1998).
- [33] P. L. Hagelstein and D. R. Denison, Nearly isotropic photonic bandgap structures in two dimensions, *Optics Letters* **24**, 708 (1999).
- [34] A. Della Villa, S. Enoch, G. Tayeb, V. Pierro, V. Galdi, and F. Capolino, Band gap formation and multiple scattering in photonic quasicrystals with a penrose-type lattice, *Physical Review Letters* **94**, 183903 (2005).
- [35] A. Shih, M. Casiulis, and S. Martiniani, Fast Generation of Spectrally-Shaped Disorder, *Physical Review E* **110**, 034122 (2024).
- [36] D. Levine and P. J. Steinhardt, Quasicrystals: A new class of ordered structures, *Physical Review Letters* **53**, 2477 (1984).
- [37] See Supplemental Material at [URL\\_will\\_be\\_inserted\\_by\\_publisher](#) for a comparison between structure factors of known bandgap formers and gyromorphs, detailed numerical methods, a full characterization of the peak height in gyromorphs against  $G$ , further discussions about the sum of cosine function that approximates  $g(r)$ , a reminder of the derivation of relevant quantities and equations within the coupled dipoles method, additional scalings for the bandgap quality against physical parameters, and the equivalent of the main text results for  $2d$  and  $3d$  scalar waves.
- [38] N. De Bruijn, Algebraic theory of Penrose's non-periodic tilings of the plane. I, II : dedicated to G. Pólya, *Indagationes Mathematicae* **43**, 39 (1981).
- [39] N. de Bruijn, Quasicrystals and their Fourier trans-

- form, *Indagationes Mathematicae (Proceedings)* **89**, 123 (1986).
- [40] M. Lax, Multiple Scattering of Waves, *Reviews of Modern Physics* **23**, 287 (1951).
- [41] M. Lax, Multiple scattering of waves. II. the effective field in dense systems, *Physical Review* **85**, 621 (1952).
- [42] R. Carminati and J. C. Schotland, *Principles of Scattering and Transport of Light* (Cambridge University Press, 2021).
- [43] P. J. Steinhardt, D. R. Nelson, and M. Ronchetti, Bond-orientational order in liquids and glasses, *Physical Review B* **28**, 784 (1983).
- [44] Y. F. Chen, H. C. Liang, Y. C. Lin, Y. S. Tzeng, K. W. Su, and K. F. Huang, Generation of optical crystals and quasicrystal beams : Kaleidoscopic patterns and phase singularity, *Physical Review A* **83**, 053813 (2011).
- [45] P.-H. Tuan and L.-Q. Huang, Optical vector fields with kaleidoscopic quasicrystal structures by multiple beam interference, *Optics Express* **31**, 33077 (2023).
- [46] Y. Rosenfeld, Free-energy model for the inhomogeneous hard-sphere fluid in D dimensions: Structure factors for the hard-disk (D=2) mixtures in simple explicit form, *Physical Review A* **42**, 5978 (1990).
- [47] P. P. Ewald, Die Berechnung optischer und elektrostatischer Gitterpotentiale, *Annalen der Physik* **369**, 253 (1921).
- [48] C. Kittel, *Introduction to Solid-state Physics* (John Wiley & Sons, New York, 1953).
- [49] A. F. Oskooi, D. Roundy, M. Ibanescu, P. Bermel, J. D. Joannopoulos, and S. G. Johnson, Meep: A flexible free-software package for electromagnetic simulations by the FDTD method, *Computer Physics Communications* **181**, 687 (2010).
- [50] A. Yamilov, S. E. Skipetrov, T. W. Hughes, M. Minkov, Z. Yu, and H. Cao, Anderson localization of electromagnetic waves in three dimensions, *Nature Physics* **19**, 1308 (2023).
- [51] M. Casiulis, A. Shih, and S. Martiniani, Materials Analysis via Greene Tensors (MAGreeTe) (2024).
- [52] O. Leseur, R. Pierrat, J. J. Sáenz, and R. Carminati, Probing two-dimensional Anderson localization without statistics, *Physical Review A - Atomic, Molecular, and Optical Physics* **90**, 053827 (2014).
- [53] O. Leseur, R. Pierrat, and R. Carminati, High-density hyperuniform materials can be transparent, *Optica* **3**, 763 (2016).
- [54] The reason for not measuring the transmission in the far field is that the monochromatic Gaussian beam is not in fact a physical laser beam, in the sense that its intensity does not decay according to the Rayleigh-Sommerfeld boundary condition in the far field [42].
- [55] R. Pierrat and R. Carminati, Spontaneous decay rate of a dipole emitter in a strongly scattering disordered environment, *Physical Review A - Atomic, Molecular, and Optical Physics* **81**, 063802 (2010).
- [56] V. H. Lutfalla, An effective construction for cut-and-project rhombus tilings with global n-fold rotational symmetry, in *27th IFIP WG 1.5 International Workshop on Cellular Automata and Discrete Complex Systems (AUTOMATA 2021)*, 9, edited by A. Castillo-Ramirez, P. Guillon, and K. Perrot (Schloss Dagstuhl – Leibniz-Zentrum für Informatik, Dagstuhl Publishing, Germany, 2021) pp. 9:1–9:12.
- [57] S. E. Skipetrov, Finite-size scaling analysis of localization transition for scalar waves in a three-dimensional ensemble of resonant point scatterers, *Physical Review B* **94**, 064202 (2016).
- [58] S. E. Skipetrov, Finite-size scaling of the density of states inside band gaps of ideal and disordered photonic crystals, *European Physical Journal B* **93**, 70 (2020).
- [59] M. Burrelli, L. Cortese, L. Pattelli, M. Kolle, P. Vukusic, D. S. Wiersma, U. Steiner, and S. Vignolini, Bright-white beetle scales optimise multiple scattering of light, *Scientific Reports* **4**, 1 (2014).
- [60] B. D. Wilts, X. Sheng, M. Holler, A. Diaz, M. Guizar-Sicairos, J. Raabe, R. Hoppe, S. H. Liu, R. Langford, O. D. Onelli, D. Chen, S. Torquato, U. Steiner, C. G. Schroer, S. Vignolini, and A. Sepe, Evolutionary-Optimized Photonic Network Structure in White Beetle Wing Scales, *Advanced Materials* **30**, 201702057 (2018).
- [61] E. van der Velden, CMasher: Scientific colormaps for making accessible, informative and 'cmashing' plots, *Journal of Open Source Software* **5**, 2004 (2020).
- [62] A. Shih, M. Casiulis, and S. Martiniani, Fast Reciprocal-Space Correlator (FReSCo) (2023).
- [63] M. Casiulis, *rusted\_core* (2023).
- [64] A. Pilleboue, G. Singh, D. Coeurjolly, M. Kazhdan, and V. Ostromoukhov, Variance analysis for Monte Carlo integration, *ACM Transactions on Graphics* **34**, 124 (2015).
- [65] E. P. Bernard, W. Krauth, and D. B. Wilson, Event-chain Monte Carlo algorithms for hard-sphere systems, *Physical Review E - Statistical, Nonlinear, and Soft Matter Physics* **80**, 5 (2009).
- [66] A. Cazé, R. Pierrat, and R. Carminati, Strong coupling to two-dimensional Anderson localized modes, *Physical Review Letters* **111**, 053901 (2013).

*Gyromorphs are not hyperuniform*– In the main text, we claim that gyromorphs are not hyperuniform based on results presented in Figs. 1 and 2. We present further evidence of this in Fig. 7, where we perform discrepancy measurements for disks [16, 35, 64]. To do so, we draw

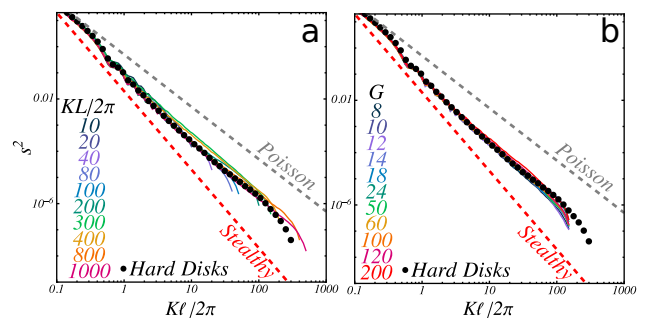


**FIG. 7. Gyromorphs are not hyperuniform.** (a) Reduced number variance from randomly drawn disks with radii  $\ell$  in 60-fold gyromorphs with various  $KL/2\pi$  from 10 to 1000 (solid colored lines), against  $K\ell/2\pi$ , in log-log scale. A dashed gray line indicates Poisson scaling,  $s^2 \sim \ell^{-d}$ , and a dashed red line the stealthy scaling  $s^2 \sim \ell^{-d-1}$ . Black disks indicate data from equilibrium hard disks with a  $\phi = 0.6$  filling fraction, for which the  $x$  axis has been rescaled using the location of the first peak as a  $K$  value. (b) Similar plot but varying the order of rotational symmetry  $G$  for  $KL/2\pi$ .

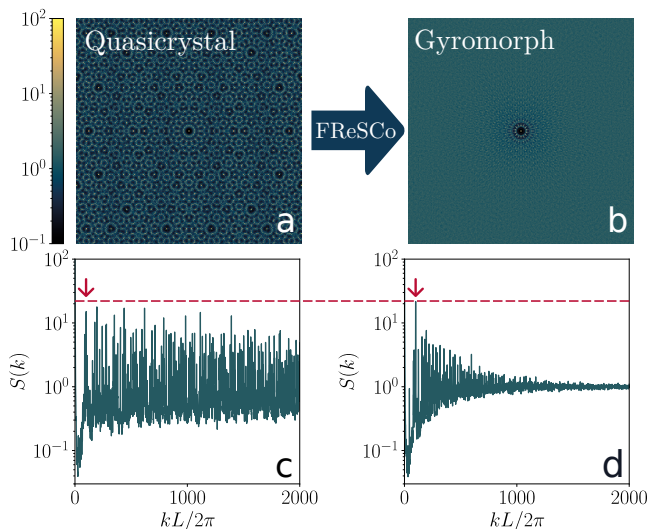


FIG. 8. **Gyromorph generated from a Quasicrystal.**  $2d$  structure factors of (a) a 14-fold quasicrystal and (b) a 14-fold gyromorph generated using the quasicrystal as an initial condition. (c), (d) depict radial structure factors of the quasicrystal and gyromorph respectively.

random disks with radius  $\ell$  at uniform positions within 60-fold gyromorphs and count the number of points that each disk contains. We then measure the mean number  $\mu$  and the variance  $\sigma^2$  of this number using 10,000 disks, and compute the reduced variance  $s^2 \equiv \sigma^2/\mu^2$  for each  $\ell$ . The output is shown when varying  $K$  for  $G = 60$  in Fig. 7(a), where  $s^2$  is plotted against  $K\ell/2\pi$  in logarithmic scales. We show that gyromorphs display number fluctuations close to Poissonian ( $s^2 \sim \ell^{-d}$ ) at small length scales, then feature sub-Poissonian fluctuations at ranges larger than  $1/K$ . While the behaviour is non-Poissonian, the slope is much weaker than that of stealthy hyperuniform systems ( $s^2 \sim \ell^{-d-1}$ ). In fact, we show that gyromorphs are near-indistinguishable from equilibrium hard disk liquids, using data from an  $N \sim 10^5$  equilibrium configuration obtained by Event-Chain Monte Carlo [65]. This conclusively shows that gyromorphs are *not* hyperuniform, even in the largest systems we test,  $N \sim 10^6$ . We show in Fig. 7(b) that this result holds when scanning values of  $G$  at a fixed  $K$ , even at rotational symmetries of order as low as 8-fold, where gyromorphs may more easily be confused [35] with quasicrystals (which follow the stealthy scaling [16]).

*Gyromorphs and Quasicrystals* – We here further discuss the differences and commonalities between gyromorphs and quasicrystals. First, we produce a 14-fold quasicrystal by de Bruijn’s method [38, 39], and report its  $S(k)$  in Fig. 8(a), (c), respectively as an intensity map in  $k$ -space and as a radially-averaged function of  $k$ . The structure factor is patterned up to very large  $k$ , resulting in peaks with near-constant (but slowly decaying) intensity in the radial plot. We use this structure as an initial

condition for our algorithm, aiming to enhance the height of the existing first ring of high quasicrystalline peaks (indicated by the arrow in Fig. 8(b)). The result, whose  $S(k)$  is shown in Fig. 8(b), (d) is indistinguishable from what we obtain from random initial conditions. In particular, note that the large- $k$  structure in  $S$  is completely destroyed: the far-away pattern has been “pumped” into the peaks to make them (about 3 times) higher, as highlighted by a red dashed line. This experiment shows that gyromorphs, the minima of our loss function, are not simply noisy quasicrystals but do in fact display stronger peaks even at small  $G$ . Furthermore, gyromorphs are not simply entropically more favorable than quasicrystals, they actually better minimize our loss function.

This difference becomes starker at larger orders of rotational symmetry, as the height of the  $S(k)$  peaks of de Bruijn quasicrystals decays fast with  $G$  [10]. However, we highlight an interesting link between gyromorphs and quasicrystals in Fig. 9, where we show side-by-side comparisons of these two quantities for  $G = 100$  in panels Fig. 9(a), (c), and  $G = 14$  in panels Fig. 9(b), (d). All systems were made using  $N \approx 10^4$  points. The quasicrystals are constructed using de Bruijn’s multigrid and dual method [38, 39, 56]. The panels show near-perfect agreement between the real (resp. reciprocal) features of gyromorphs and the reciprocal (resp. real) features of quasicrystals. In other words, gyromorphs look like duals of quasicrystals. This is because the  $S(k)$  of gyromorphs (resp. the  $g(r)$  of quasicrystals) is dominated by one ring of high peaks, so that its Fourier transform is

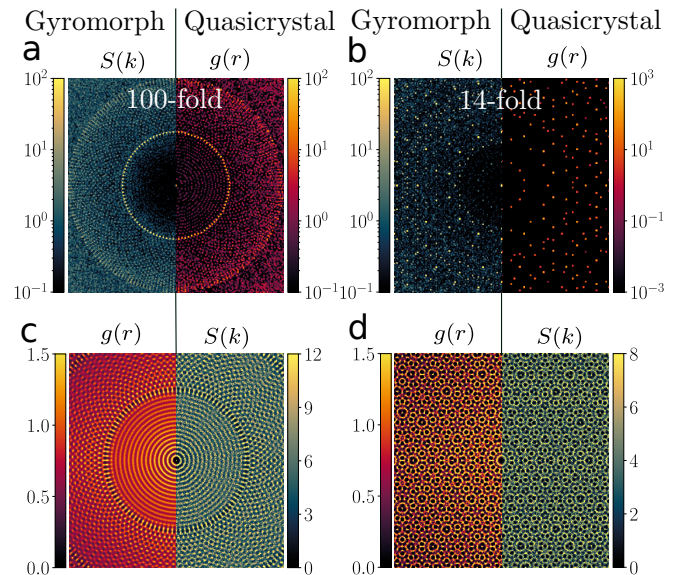


FIG. 9. **Gyromorphs as duals of Quasicrystals.** Comparisons between the  $S(k)$  (resp.  $g(r)$ ) of  $2d$  gyromorphs and the  $g(r)$  (resp.  $S(k)$ ) of quasicrystals for (a), (c)  $G = 100$  and (b), (d)  $G = 14$ . The plot ranges and intensity scales are adjusted to match images.

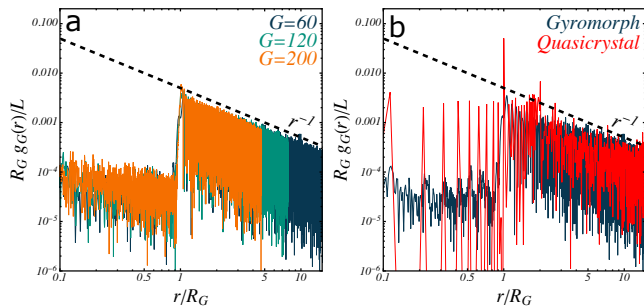


FIG. 10. **Rotational order in gyromorphs.** Gyromorphic correlation function  $g_G$ , rescaled by  $R_G/L$ , against  $r/R_G$ , for  $G = 60$  (dark blue),  $G = 120$  (green),  $G = 200$  (orange). A dashed black line shows a  $r^{-1}$  power law as a guide for the eye. Here,  $KL/2\pi = 300$ .

well approximated by a sum of cosines.

To highlight that gyromorphs display quasi-long-range rotational order, in Fig. 10(a), we plot a gyromorphic correlation function,  $g_G$ , defined as

$$g_G(r) \equiv \left| \frac{L^d}{N^2} \frac{1}{2\pi} \sum_{p \neq q} e^{in\theta_{pq}} \delta(r - r_{pq}) \right|, \quad (1)$$

where the sum runs over all pairs of particles, that are separated by a distance vector  $\mathbf{r}_{pq}$  with polar components  $(r_{pq}, \theta_{pq})$ . That is essentially the value of the modulus of the  $G$ -th Fourier mode of a shell of  $g(r)$  at distance  $r$ . When suitably rescaled by  $R_G$ , this function collapses across values of  $G$ , and displays a power-law decay with an exponent close to  $-1$ . We show in Fig. 10(b) a comparison of that function between a  $G = 60$  gyromorph and the corresponding quasicrystal, with  $R_G$  taken as the location of the strongest peak. The difference is mainly that quasicrystals display strong rotational order with nearest neighbors, as they lie on a discrete set of orientations along a rhombic tiling, while gyromorphs are isotropic at short range. The long-range behavior, however, is nearly the same. Thus, gyromorphs display quasi-long-range rotational order, that extends throughout the system [35, 37].

*Coupled dipoles in a nutshell* – If  $\mathbf{r}_i$  represents the position of scatterer  $i$ ,  $\mathbf{E}_{inc}(\mathbf{r}_i; \omega)$  is the  $\omega$ -component of the Fourier representation of an arbitrary incident field at  $\mathbf{r}_i$  and  $\mathbf{E}(\mathbf{r}_i; \omega)$  is the total exciting field at scatterer  $i$ , this system can be written as

$$\mathcal{M}(\{\mathbf{r}_{ij}\}; \omega) \cdot \mathcal{E}(\{\mathbf{r}_j\}; \omega) = \mathcal{E}_{inc}(\{\mathbf{r}_i\}; \omega), \quad (2)$$

where we introduced rank-2 tensor notations for the values of both kinds of fields so that for instance  $\mathcal{E}_{i,a} = \mathbf{E}(\mathbf{r}_i; \omega) \cdot \hat{\mathbf{e}}_a$  with  $a \in \{x, y, z\}$ , and  $\mathcal{M}(\{\mathbf{r}_{ij}\}; \omega)$  is rank-4 with elements

$$\mathcal{M}_{ijab} = \begin{cases} \delta_{ab}(1 - k_0^2 \alpha(\omega) \Sigma) & \text{if } i = j \\ -k_0^2 \alpha(\omega) \hat{\mathbf{e}}_a \cdot \overline{\mathbf{G}}_0(\mathbf{r}_i, \mathbf{r}_j; \omega) \cdot \hat{\mathbf{e}}_b & \text{otherwise.} \end{cases} \quad (3)$$

In this last expression,  $\alpha(\omega) \equiv V\delta\varepsilon$  is the polarizability of a scatterer with volume  $V$ ,  $\Sigma$  is a self-interaction term that ensures energy conservation and  $\overline{\mathbf{G}}_0$  is the Green tensor of free propagation with the desired boundary conditions (here, Rayleigh-Sommerfeld ones [42]). Solving Eq. 2 for vector waves with  $p$  components reduces to a  $pN \times pN$  linear solve yielding  $\mathcal{E} = \mathcal{W} \cdot \mathcal{E}_{inc}$  where  $\mathcal{W} = \mathcal{M}^{-1}$ . From that solution, the full electromagnetic field at any position  $\mathbf{r}$  outside of scatterers can be reconstructed as

$$\mathbf{E}(\mathbf{r}; \omega) = \mathbf{E}_{inc}(\mathbf{r}; \omega) + k_0^2 \alpha(\omega) \mathcal{G}_0(\mathbf{r}, \{\mathbf{r}_i\}; \omega) \cdot \mathcal{E}(\{\mathbf{r}_i\}; \omega), \quad (4)$$

where  $\mathcal{G}_0$  is a rank-3 tensor with elements  $\mathcal{G}_{0,iab} = \hat{\mathbf{e}}_a \cdot \overline{\mathbf{G}}_0(\mathbf{r}, \mathbf{r}_i; \omega) \cdot \hat{\mathbf{e}}_b$ . In practice, we use

$$\mathbf{E}_{inc}(\mathbf{r}; \omega) \equiv \mathbf{E}_0 \exp \left[ -i\mathbf{k}_0 \cdot \mathbf{r}_{\parallel} - \frac{r_{\perp}^2}{w^2} \right], \quad (5)$$

with  $\mathbf{r}_{\parallel}, \mathbf{r}_{\perp}$  the components of  $\mathbf{r}$  parallel and perpendicular to a beam with width  $w = L/5$ , respectively. Finally, to assert the presence of bandgaps, we compute the local density of optical states (LDOS)

$$\varrho(\mathbf{r}; \omega) \equiv \frac{2\omega}{\pi c^2} \text{Im Tr}_p \overline{\mathbf{G}}(\mathbf{r}, \mathbf{r}; \omega). \quad (6)$$

The coupled dipoles method lets us compute the relative change of LDOS compared to the vacuum value,  $\delta\varrho = \varrho/\varrho_0 - 1$ , as the trace of a tensor product.

$$\delta\varrho(\mathbf{r}; \omega) = C_p \text{Im} \left[ \alpha \text{Tr}_p \left[ \mathcal{G}_0(\mathbf{r}; \{\mathbf{r}_i\}) \cdot \mathcal{W} \cdot {}^t \mathcal{G}_0(\mathbf{r}; \{\mathbf{r}_j\}) \right] \right], \quad (7)$$

where we dropped the  $\omega$  dependence from the tensor notations for compactness and  $C_p = (2\omega^3)/[\pi c^4 \varrho_0(\omega)]$ . Following past works [14, 55, 66], we estimate the DOS of the medium at points at least  $2a$  away from scatterer centers, and average the result over random points in the medium. We remind the standard [42] derivation of these equations and the precise definitions of every term in 2d and 3d in SM [37].